

# The Role of Short-Range Order and Hyperuniformity in the Formation of Band Gaps in Disordered Photonic Materials

Luis S. Froufe-Pérez,<sup>1</sup> Michael Engel,<sup>2,3</sup> Pablo F. Damasceno,<sup>2,3</sup> Nicolas Muller,<sup>1</sup> Jakub Haberko,<sup>4</sup> Sharon C. Glotzer,<sup>2,3,5</sup> and Frank Scheffold<sup>1</sup>

<sup>1</sup>*Department of Physics, University of Fribourg, CH-1700 Fribourg, Switzerland*

<sup>2</sup>*Department of Chemical Engineering, University of Michigan, Ann Arbor, Michigan 48109, USA*

<sup>3</sup>*Biointerfases Institute, University of Michigan, Ann Arbor, Michigan 48109, USA*

<sup>4</sup>*Faculty of Physics and Applied Computer Science,*

*AGH University of Science and Technology, 30-059 Krakow, Poland*

<sup>5</sup>*Department of Materials Science and Engineering,*

*University of Michigan, Ann Arbor, Michigan 48109, USA*

## GENERATION OF POINT PATTERNS

The point patterns used as seeds for the generation of photonic structures are obtained using numerical simulation and optimization. Simulation codes for this work are written in C++ and included as Supplemental Material.

Hard disk (HD) patterns are snapshots from isochoric Monte Carlo simulations of hard disks with radius  $R$  in a box of area  $A$  and with periodic boundary conditions. Important parameters are the number of particles  $N$  and the packing density  $\phi = N\pi R^2/A$ . A disordered starting configuration is rapidly compressed to the target density and then equilibrated. A short equilibration time over  $10^4$  Monte Carlo sweeps proved already sufficient to reach equilibrium.

Stealthy hyperuniform (SHU) patterns are the final configuration from molecular dynamics runs of a system of particles interacting with an appropriate pair potential. We follow Ref. [1] and choose as potential energy

$$E = \sum_{|\mathbf{k}| \leq K} S(\mathbf{q}) = \frac{1}{N} \sum_{|\mathbf{k}| \leq K} \left\| \sum_{j=1}^N e^{-i\mathbf{k} \cdot \mathbf{R}_j} \right\|^2, \quad (1)$$

where  $\mathbf{R}_j$  is the position of the  $j$ -th particle. The force is derived as

$$\mathbf{F}_l = -\frac{\partial E}{\partial \mathbf{R}_l} = \frac{1}{N} \sum_{|\mathbf{k}| \leq K} \mathbf{k} \operatorname{Im} \left( \sum_j e^{i\mathbf{k} \cdot (\mathbf{R}_l - \mathbf{R}_j)} \right), \quad (2)$$

which simplifies to

$$\mathbf{F}_l = \frac{1}{N} \sum_{|\mathbf{k}| \leq K} \mathbf{k} (C \sin(\mathbf{k} \cdot \mathbf{R}_l) - S \cos(\mathbf{k} \cdot \mathbf{R}_l)), \quad (3)$$

with  $C = \sum_j \cos(\mathbf{k} \cdot \mathbf{R}_j)$  and  $S = \sum_j \sin(\mathbf{k} \cdot \mathbf{R}_j)$ . The sum runs over points in reciprocal space corresponding to the reciprocal lattice defined by the simulation box. The potential is long-range, with SHU patterns as ground states. Note that the potential assumes a Bessel function in the limit of  $N \rightarrow \infty$  due to the relation

$$\int_{|\mathbf{k}| \leq K} \mathbf{k} e^{i\mathbf{k} \cdot \mathbf{r}} d^2 \mathbf{k} = 2\pi \frac{K\mathbf{r}}{r^2} J_1(Kr). \quad (4)$$

We construct SHU patterns by simulated annealing over  $10^4$  molecular dynamics time steps. The annealing starts from a random configuration and follows a logarithmic ramp for the kinetic energy using an Andersen thermostat in the range  $10^{-1} \leq E_{\text{kin}} \leq 10^{-7}$ . The constraint parameter  $\chi$  is defined as

$$\chi = \frac{\#\text{constrained } \mathbf{k}}{d(N-1)}, \quad (5)$$

where  $d = 2$  is the dimensionality and the number of constrained  $\mathbf{k}$  is the number of terms in the sum in Eq. (1). If we cannot achieve a target  $\chi$  with a given  $N$ , then  $N$  is adjusted to the closest value that is compatible with that  $\chi$ .

We generally use  $N = 200$  and vary  $0.1 \leq \phi \leq 0.75$  and  $0.1 \leq \chi \leq 0.75$ . Example snapshots at various parameter values are shown in Fig. 1. However, in contrast to the rest of the paper we used  $N = 1000$  in the snapshots to highlight the development of order with increasing positional correlation. The HD system crystallizes into a hexagonal lattice in the density range  $0.70 < \phi < 0.72$ . The SHU system orders over the broad density range  $0.50 < \chi < 0.70$ , gradually changing from hexagonal (six-fold) local order to four-fold local order with increasing density. Interestingly, the ordered phase of the SHU system appears to be the square lattice, albeit typically with defects. It is not clear whether the SHU system undergoes a first order phase transition.

The gradual appearance of order can be analyzed in real space via the radial distribution function  $g(r)$  and in reciprocal space via the structure factor  $S(k)$ . We show these functions in Fig. 2 for the patterns in Fig. 1. Notice that for better comparability at various parameter values we use a different unit of length than in Fig. 1.

Positional order gradually develops with  $\phi$  and  $\chi$  as visible by the increasing height of the peaks in  $g(r)$  and  $S(k)$ . At  $\phi, \chi \geq 0.70$ , additional peaks appear indicating the development of quasi-long-range order. While the second peaks of the fluid splits up in the HD system, indicating the formation of a hexagonal lattice, a new peak develops for the SHU patterns. This peak is at a posi-

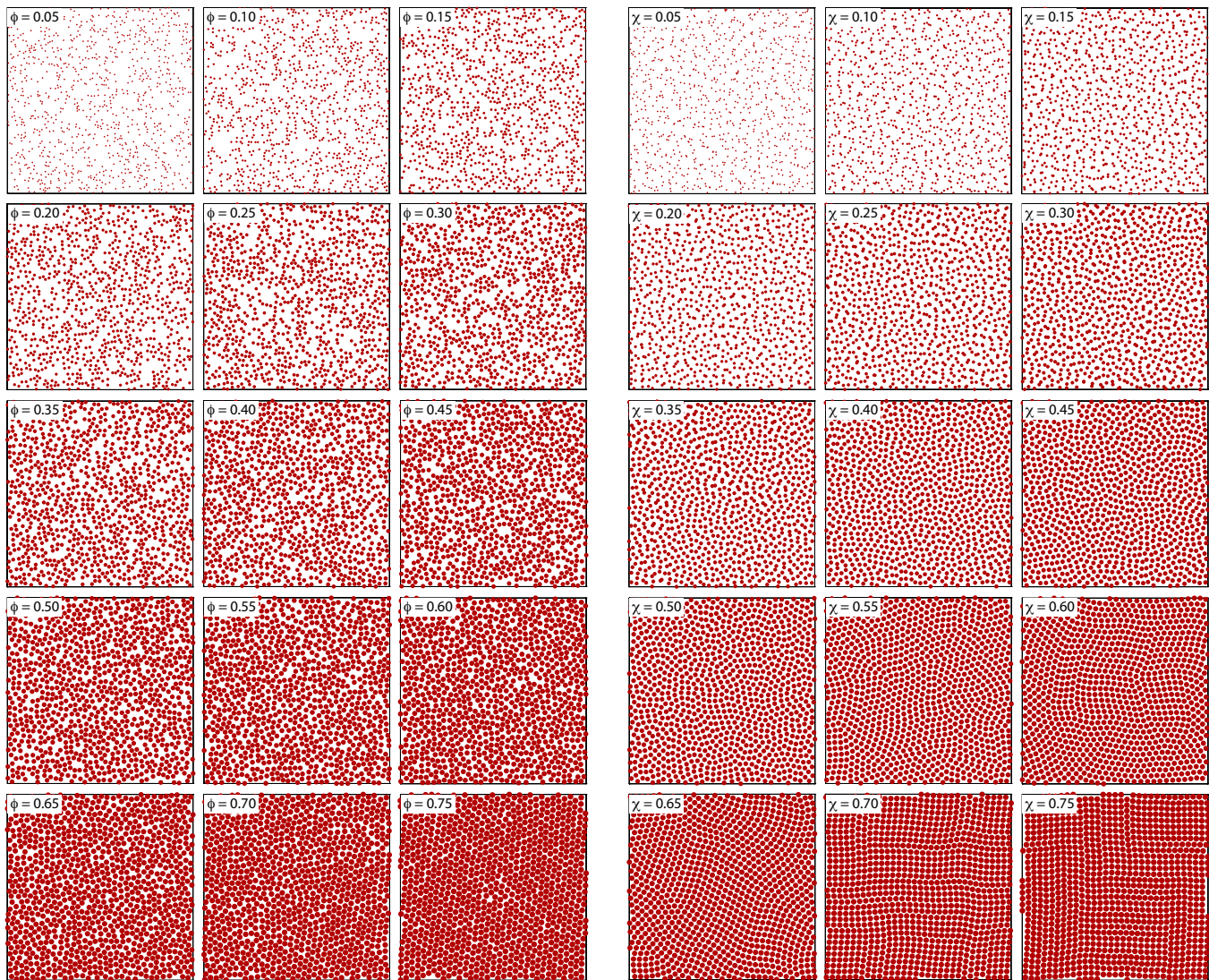


FIG. 1. Example HD snapshots (left) and SHU snapshots (right). Both systems order gradually with increasing correlation parameter  $\phi$  and  $\chi$ . Points in the patterns are drawn as disks. To allow a better comparison between HD and SHU patterns, the radius  $R$  of the disk in the SHU patterns is chosen such that  $\chi = \pi R^2 N/A$ .

tion of about  $\sqrt{2}$  compared to the first peak, indicating the formation of a square crystal. While there is a discontinuity in  $g(r)$  at  $r = R$  with increasing height for HD patterns, there is only a weak discontinuity in  $S(k)$  at  $k = K$  for SHU patterns. Apparently scattering is ‘pushed back’ in the SHU system to higher  $k$ -values in order to allow for an even larger  $k$  gap than necessary by the stealthiness condition.

### PHOTONIC BAND STRUCTURE CALCULATIONS

All photonic band structure calculations are performed with the open source code MIT Photonic Bands [2]. We use the material silicon (dielectric constant  $\epsilon = 11.6$ ).

The path in reciprocal space follows the boundary of the irreducible part of the first Brillouin zone of the hexagonal lattice,  $\Gamma-M-K-\Gamma$  and along the path  $\Gamma-X-M-\Gamma$  for the square superlattice.

### Crystalline structures

The densest packing of hard disks (HDs) is the hexagonal lattice with packing density  $\phi_{\max} = \pi/\sqrt{12} \simeq 0.91$ . We compare this limiting case with the disordered structures. We also use the hexagonal lattice to optimize the geometric parameters of the silicon rods and walls.

The silicon rod radius for the transverse-magnetic (TM) case,  $r/a = 0.189$ , was considered optimal in [3] [Fig. 3(left)].

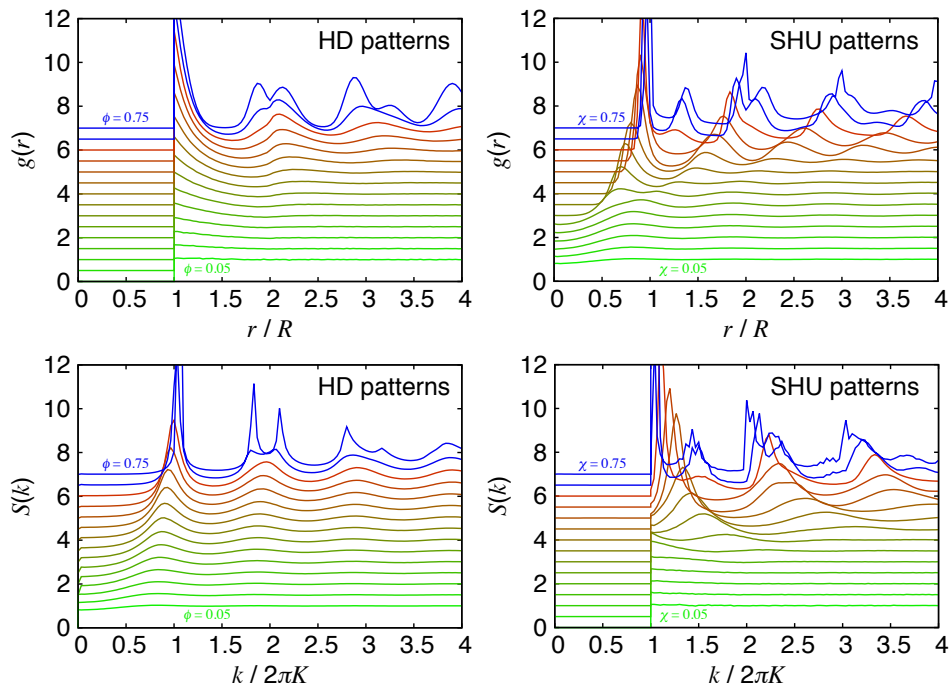


FIG. 2. Radial distribution function  $g(r)$  and structure factors  $S(k)$  of HD point patterns (left) and SHU point patterns (right) as a function of  $\phi$  and  $\chi$ , respectively. The color gradually changes from green to red as the positional correlation increases. Snapshots with  $\phi, \chi \geq 0.7$ , which are mostly ordered, are colored blue. With each increase by  $\Delta\phi = \Delta\chi = 0.05$ , curves were shifted vertically by 0.5 for better separation. Every curve is the result of an averaging over 1000 statistically independent patterns.

When the protocol used to generate the trivalent network is applied to a hexagonal lattice, the honeycomb lattice is retrieved. We optimize the geometric parameter of the honeycomb lattice to maximize the photonic band gap (PBG) width in transverse-electric (TE) polarization. The wall thickness corresponding to the widest PBG is  $w/a = 0.288$  [Fig. 3(middle)].

To open overlapping full PBGs for both polarizations simultaneously, we consider a decorated network, which combines rods and the network. We optimize the geometric parameters of the decorated honeycomb lattice in order to maximize the joint PBG width. The parameters corresponding to the widest PBG are  $w/a = 0.0593$  and  $r/a = 0.2275$  [Fig. 3(right)].

In Fig. 4a we present a colormap of the relative width of the overlapping gaps in TE and TM polarizations as a function of the geometrical parameters of the decorated network. The circle in this figure represents the chosen parameters in this work for the decorated network. The shaded area represents decorated networks where the cylinder is fully embedded into the walls. In Fig. 4b we show the complete PBG relative width as a function of the wall thickness. As can be seen here, it is possible to open a complete but narrow PBG using a non-decorated honeycomb lattice. Nevertheless its maximum width is only 1.2% and the gap will have a negligible width after introducing even small amounts of disorder.

### Disordered structures

We apply the supercell method [4], which considers a square piece of the disordered structure as the primitive cell of a periodic lattice. To avoid spurious states related to the surface termination that can populate the otherwise clean PBG, it is necessary to generate seed point patterns using periodic boundary conditions matching the geometry of the supercell. The minimum number of bands that need to be calculated depends on the number of scattering units  $N$  in the supercell and on the polarization. In all the considered cases, our seed point patterns contain  $N \simeq 200$  points. The MPB calculations are done setting the resolution to  $a/32$  and the tolerance in frequency to  $10^{-4}$ , which is sufficient to resolve the spectral properties of our systems. In Fig. 5 we compare the structure factor of the single MPB samples (derived from the point patterns shown in Fig. 1a and 1c in the main text). We first compute analytically the full structure factor by multiplying  $S(k)$  of the point pattern (HD and SHU) with the form factor  $F(k)$  of a circle with  $r/a = 0.189$ . We then divide the result by the square of the surface of the cylinder,  $s = \pi r^2$  (open circles in Fig 5). Next we compute the two dimensional Fourier transform of the discretized structure as generated by the MPB software. Computing the angular average we obtain (again after scaling by  $s^{-2}$ ) the corresponding  $S(k)$ ,

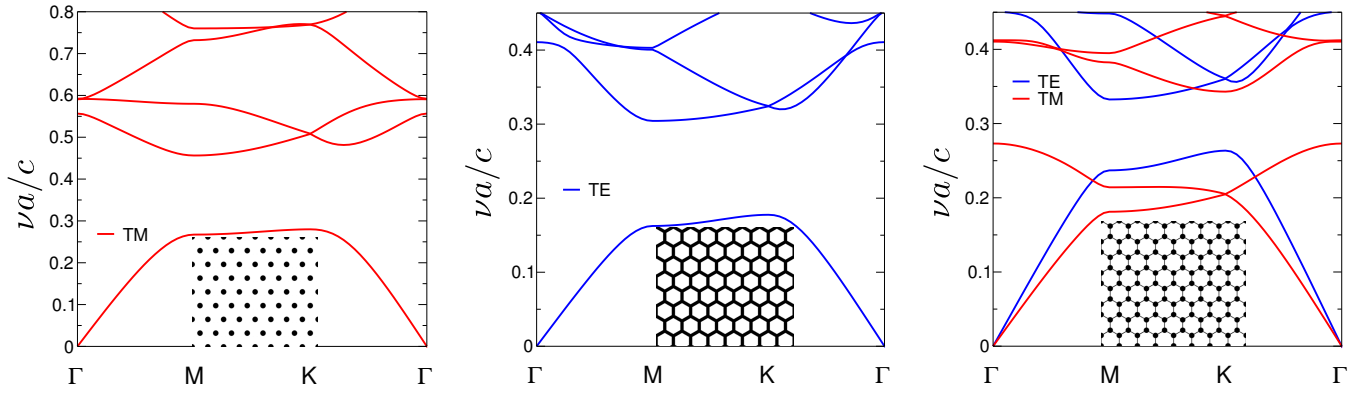


FIG. 3. Photonic band structure in various polarizations. The insets shows the permittivity function in real space. (left) TM polarization for a hexagonal lattice of silicon rods (radius  $r/a = 0.189$ ). The full PBG opens between the first and the second bands and the relative width is  $\Delta\nu/\nu_0 = 47.9\%$ . No PBG is found in TE polarization. (middle) TE polarization for a honeycomb lattice of silicon walls (thickness  $w/a = 0.288$ ). The full PBG opens between the first and the second bands and the relative width is  $\Delta\nu/\nu_0 = 52.6\%$ . No PBG is found in TM polarization. (right) Honeycomb lattice of silicon walls decorated with rods (radius  $r/a = 0.2275$ ) at network nodes (wall thickness  $w/a = 0.0593$ ). The full PBG opens between the first and the second bands in both polarizations and the relative width is  $\Delta\nu/\nu_0 = 19.6\%$ .

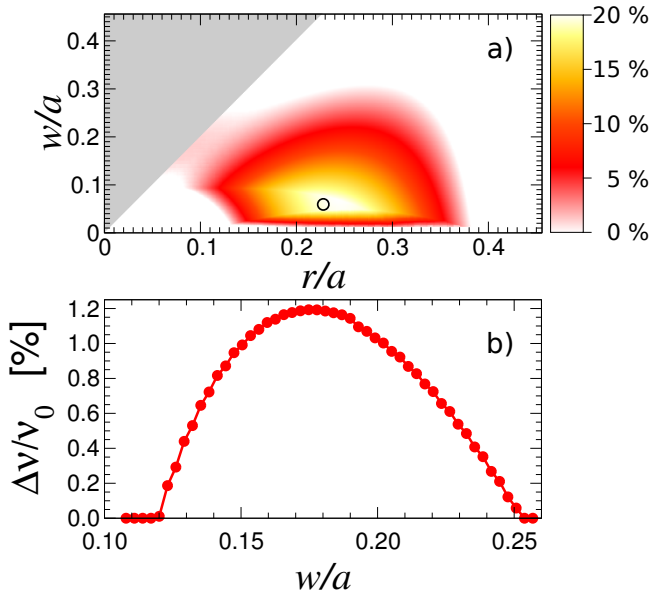


FIG. 4. (a) Colormap of the full (TE and TM) PBG relative width as a function of the geometrical parameters  $r/a$  and  $w/a$ . In the shaded area the relationship  $r < w/2$  holds. (b) Full PBG width as a function of  $w/a$  for non-decorated honeycomb lattices.

shown as crosses in Fig. 5. Despite some visible difference in the log-plot due to discretization we find that the agreement between the analytic (circles) and fully numerical (crosses) structure factors is good. In particular the MPB discretized structure retains the SHU character and shows a drop by more the four orders of magnitude in  $S(k)$  for  $ka/2\pi < 0.5$ .

From the band diagrams [Fig. 6 and Fig. 7] we obtain the precise position of the band edges and also the effective

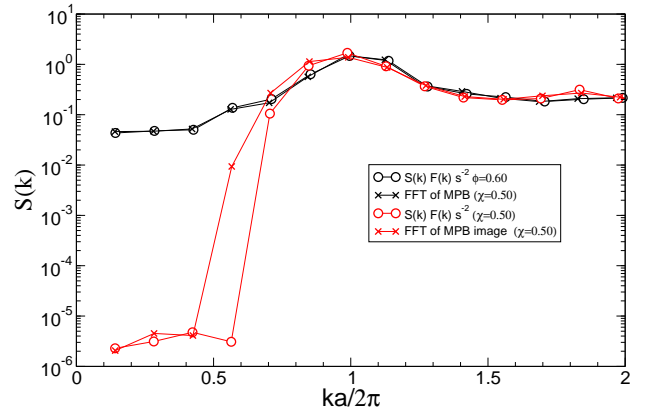


FIG. 5. Structure factors (considering both position and size of the rods and normalized by the square of the surface of the rods) for the HD (black) and SHU (red) patterns considered in Fig. 1a and Fig. 1c. We compare the analytical (open circles) and the fully numerical (crosses) structure factors as explained in the text.

refractive index  $n_{\text{eff}}$  of the medium at low frequency. To determine  $n_{\text{eff}}$  we apply two approaches: (i) fitting the lowest band (solid lines in the figures) to the dispersion relation of a homogeneous medium, and (ii) the Maxwell-Garnett mixing rule. In general, the two methods give values for  $n_{\text{eff}}$  that differ by less than 2% for all examined cases.

In the case of TM polarization [Fig. 6] according to the Maxwell-Garnett rule the effective permittivity for rods of filling fraction  $\phi_0$  in vacuum is  $\epsilon_{\text{eff}} = n_{\text{eff}}^2 = (\epsilon_{\text{rods}} - 1)\phi_0 + 1$ . With the present parameters we obtain  $n_{\text{eff}} \simeq 1.48$ .

If we compare the band structure for TM polarization

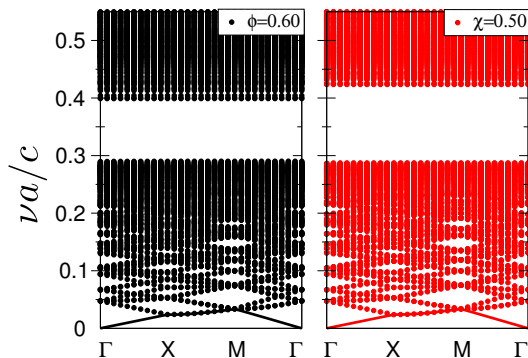


FIG. 6. Photonic band structure for systems composed of  $N = 200$  silicon rods (radius  $r/a = 0.189$ ) in TM polarization. The rods are positioned according to the HD model with  $\phi = 0.60$  (left) and the SHU model with  $\chi = 0.50$  (right), *i.e.* the case discussed in Figs. 1-3. We calculate  $2N$  bands. The PBG opens between the bands  $N$  and  $N + 1$ . Solid lines indicate the lowest frequency band used to obtain the refractive index of the effective medium.

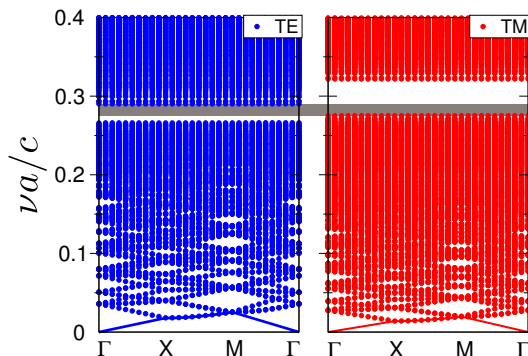


FIG. 7. Photonic band structure for a decorated trivalent network of silicon rods ( $r/a = 0.2275$ ) and walls ( $w/a = 0.0593$ ) derived from a  $N = 200$  HD seed pattern with  $\phi = 0.60$ . We calculate  $3N$  bands in TE polarization (left) and TM polarization (right). For TE modes, the PBG opens between the bands  $N$  and  $N + 1$ , while for TM modes the PBG lies between the bands  $2N$  and  $2N + 1$ . Solid lines indicate the lowest frequency band used to obtain the refractive index of the effective medium. The shaded stripe occupies the frequency range in which PBGs for both polarizations overlap.

[Fig. 6] with the band structure for the decorated honeycomb [Fig. 7], we see a close correspondence in the position of the PBG for both polarizations. While the first TE PBG opens between the first and second bands for the decorated honeycomb (corresponding to the  $N$  and  $N + 1$  bands in the supercell), the first TM PBG opens between the second and the third bands in the decorated honeycomb, (corresponding to the  $2N$  and  $2N + 1$  bands in the superlattice). This is a rather general behavior found for all values of  $\chi \gtrsim 0.2$  and  $\phi \gtrsim 0.2$ . The trend is not followed for smaller parameter values.

## Normalized density of states

A full calculation of the photonic density of states (DOS) requires a massive sampling in reciprocal space. Such a sampling for a complex supercell geometry and band counts reaching several hundreds can be prohibitively slow, even when using relatively large computational facilities, which makes it difficult to systematically scan the  $\chi$  and  $\phi$  parameters. In order to alleviate the required computational efforts, we note that the band structure close to the band edges in the supercell method is nearly flat. This fact suggests that it is sufficient to use a comparably sparse sampling grid in reciprocal space when calculating the DOS. Hence, we sample along the  $\Gamma - X - M - \Gamma$  path (of the square lattice in the supercell method) with only 31 points.

We compute a frequency histogram and normalize it by the histogram that would be obtained in a homogeneous medium with refractive index given by  $n_{\text{eff}}$ . The discrete spectrum in a homogeneous medium with effective refractive index  $n_{\text{eff}}$  at each  $\mathbf{k}$  point is given by  $\omega(\mathbf{k}, \mathbf{G}) = c|\mathbf{k} + \mathbf{G}|/n_{\text{eff}}$  for all reciprocal lattice vectors  $\mathbf{G}$  of the super lattice. The histogram used to normalize is built by considering all the eigenfrequencies of the homogeneous medium spectrum at each of the sampling points in the reciprocal space used in the band structure calculation of the disordered systems. This procedure gives the normalized DOS (nDOS) that is presented in the main text. The nDOS is a convenient way of integrating the information contained in the full band structure and provides a useful way of comparing different systems.

We study the dependence of the nDOS for HD and SHU systems on the correlation parameters  $\phi$  and  $\chi$  in TM and TE polarization separately [Fig. 8] and both polarization simultaneously [Fig. 9]. Already for low values of  $\phi$  and  $\chi$ , the nDOS is strongly depleted in the region where the PBG eventually emerges at higher correlation. Overall, the trend of the nDOS as the systems become more correlated is similar for both types of disorder and all polarizations. For high values of  $\phi$  or  $\chi$ , the nDOS resembles that of a perfect lattice: nearly flat at low frequency, followed by a peak near the PBG edge. The higher the degree of correlation in the structure, the larger the PBG width and the higher the nDOS peak near the PBG edge.

For the decorated networks we divide the obtained frequency histograms by the sum of the histograms obtained for TE and TM polarizations in a homogeneous medium with an effective refractive index that depends on polarization. In all cases shown in Fig. 9 the effective refractive indices  $n_{\text{eff}}$  in TE and TM polarization, obtained from fitting the lowest band to a homogeneous medium, vary by less than 0.5%. In particular, we have  $n_{\text{eff}}^{(TE)} = 1.395 \pm 0.004$ ,  $n_{\text{eff}}^{(TM)} = 1.799 \pm 0.009$ .

For decorated networks the full PBG is much narrower

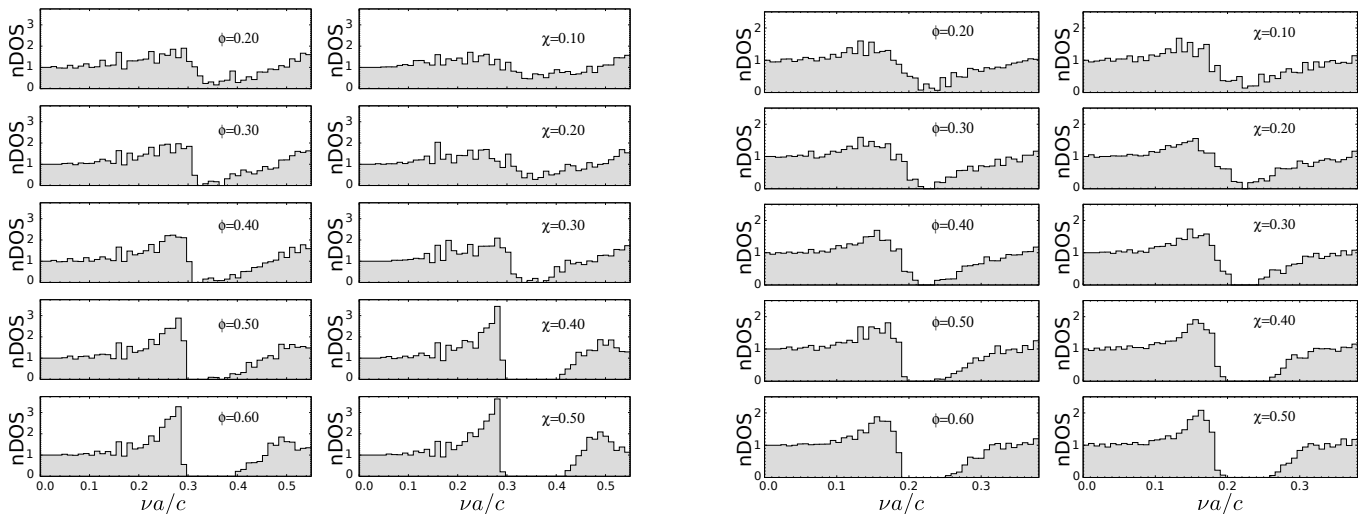


FIG. 8. (left pair) nDOS in TM polarization. The systems consist of rods obtained from HD and SHU seed patterns. (right pair) nDOS in TE polarization. The systems are trivalent networks of connected walls obtained from HD and SHU seed patterns.

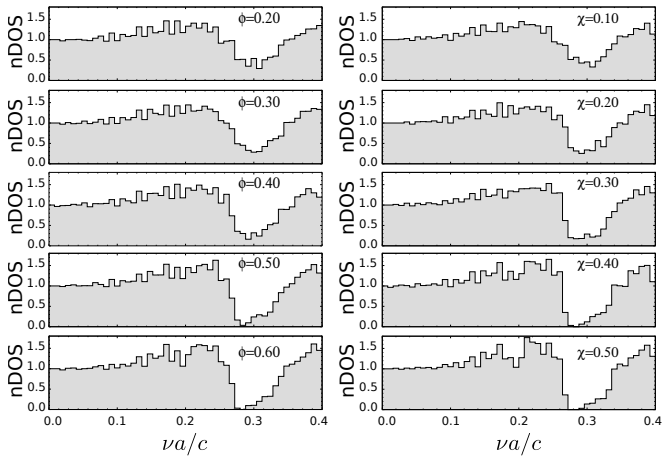


FIG. 9. Polarization-averaged nDOS for different degrees of correlations. The systems are decorated networks derived from HD (left) and SHU (right) seed patterns.

than in structures optimized solely for TM or TE polarizations. Only for a strong correlation, the PBG width is larger than the bin size of the histogram. Nevertheless, the nDOS is dramatically lowered already for weak correlations forming a pseudo-gap at the position where the full PBG eventually appears.

### Introducing defects

We introduce defects in the trivalent networks by randomly removing links with a certain probability  $p$ . We have studied the effect of link removal for the trivalent networks presented in the main text (SHU with  $\chi = 0.50$  and HD with  $\phi = 0.60$ ). To calculate the PBG we follow

exactly the same supercell method as explained above, this time with different amounts of randomly removed links. PBG data for different values of  $\chi$  (SHU) and  $\phi$  (HD) and different link removal probability  $p$  are shown in the main text.

As an illustration of the results we obtained, in Fig. 10 we plot a few of the considered cases. In Fig. 10a, the band structure obtained by the supercell method is presented together with a cartoon of the trivalent network we used. This structure is obtained after applying the triangulation protocol as explained in the main text to a SHU ( $\chi = 0.50$ ) seed pattern containing 97 points, that leads to a structure with  $N = 194$  nodes. The PBG relative width (only TE polarization) is  $\Delta\nu/\nu_0 = 28.6\%$ . The averaged value over 10 samples for a  $p = 5\%$  probability of link removal is  $\Delta\nu/\nu_0 = 10.4\%$ . In Fig. 10b,c we plot the band structure and corresponding network for the cases of widest and narrowest PBG found in the sampling,  $\Delta\nu/\nu_0 = 14.9\%$  and  $\Delta\nu/\nu_0 = 5.1\%$  respectively. A closer look on Fig. 10c suggest that the gap closes more rapidly whenever the defect affected regions form chains spanning the across whole structure, in agreement with the earlier studies on 2D crystal lattices [5].

- 
- [1] S. Torquato, G. Zhang, and F. Stillinger, *Physical Review X* **5**, 021020 (2015).
  - [2] S. Johnson and J. Joannopoulos, *Optics Express* **8**, 173 (2001).
  - [3] M. Florescu, S. Torquato, and P. J. Steinhardt, *Proceedings of the National Academy of Sciences of the United States of America* **106**, 20658 (2009), arXiv:1007.3554.
  - [4] J. D. Joannopoulos, S. G. Johnson, J. N. Winn, and R. D. Meade, *Photonic Crystals: Molding the Flow of*

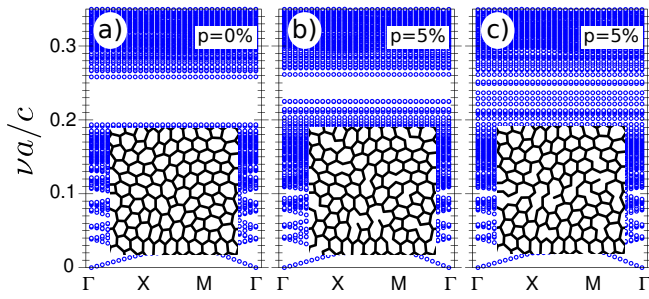


FIG. 10. Band structures in the supercell method (structures in the respective insets) for triavalent networks ( $w/a = 0.288$ ) obtained from a SHU pattern with  $\chi = 0.50$  and 97 points ( $N = 196$  nodes) for (a) none of the links are removed and (b,c)  $p = 5\%$  link removal probability. (b) corresponds to the sample with the maximum PBG width, while (c) corresponds to the sample with the minimum PBG width out of 10 samples.

*Light* (Princeton University Press, 2008).

- [5] M. Florescu, S. Torquato, and P. J. Steinhardt, *Applied Physics Letters* **97**, 201103 (2010).